Journal of Food and Agricultural Technology Research
https://globalpresspk.com/
ISSN: 3007-0953 (Online)
ISSN: 3007-0945 (Print)

Research Paper

Development and Experimental Study of a Diesel-Fired Heat Exchanger for Turmeric Drying in Pakistan

Hafiz Sultan Mahmood [a], Asif Ali Mirani [a], Badar Munir Khan Niazi [a], Hadeed Ashraf [a, *], Muzammil Husain [a] and Hafiz Md-Tahir [a]

[a] Agricultural Engineering Institute, National Agricultural Research Centre, Islamabad 44000, Pakistan

***Corresponding author:** Hadeed Ashraf (hadeedashraf@parc.gov.pk)

Abstract: Turmeric is an important spice crop in Pakistan, where post-harvest drying is essential to extend shelf life and maintain quality. Traditional open-sun and conventional hot-air drying methods are inefficient, weather-dependent, and often compromise product quality. To address these limitations, this study aimed to design, develop, and evaluate a cost-effective, diesel-fired heat exchanger integrated into a turmeric dryer. The primary objective was to assess its thermodynamic performance and operational economics for both uncrushed and crushed rhizomes, while the secondary objective was to validate experimental findings through Computational Fluid Dynamics (CFD) simulations. CFD analysis was employed to model airflow and heat transfer within the heat exchanger, providing insights into temperature distribution and aiding design optimization. Experimental results showed that the heat exchanger achieved a maximum air temperature of 96.8 °C with 1.6% relative humidity. For uncrushed turmeric, moisture content decreased from 80% to 9.67% in 30 hours, with a total moisture removal of 465.6 kg and a maximum dryer efficiency of 56.6%. The drying cost was PKR 55 per kilogram. Crushed turmeric reached 9.94% moisture in 8 hours at a cost of PKR 16 per kilogram. CFD predictions of outlet temperature closely matched experimental data, confirming model reliability, although non-uniform temperature zones were identified for future design improvements. These findings demonstrate that the developed system offers a practical, energy-efficient solution for turmeric drying in Pakistan.

Keyword: Turmeric dryer; Agricultural dryer; Design and development; Fired heat exchanger

Practical Application

- Design and development of a diesel-fired heat exchanger to improve drying time of turmeric at farm level in Pakistan.
- Up to 70% reduction in drying time and operational cost of drying crushed turmeric.
- Higher moisture take-off achieved in treatment (T2) by crushing the turmeric before drying.

Article History
Received: 2 April 2025; Revised: 9 June 2025; Accepted: 16 August 2025 Online: 07 September 2025; Published: 30 December 2025; DOI https://doi.org/10.69501/ccaqfv97
How to Cite: Mahmood, H. S., Mirani, A. A., Niazi, B. M. K., Ashraf, H., Husain, M., & Md-Tahir, H. (2025). Development and experimental study of a diesel-fired heat exchanger for turmeric drying in Pakistan. Journal of Food and Agricultural Technology Research, 4(2).

1. Introduction

Turmeric is a high-value spice whose color, aroma, and bioactive quality (notably curcuminoids) are highly sensitive to post-harvest handling and drying. Open-sun drying which is still common in South Asia, exposes rhizomes to dust, insects, and microbial contamination and can degrade curcuminoids through light and heat, producing inconsistent quality and avoidable losses (Kanwal et al. 2020; Saha et al. 2022). Controlled hot-air methods (e.g., oven or fluidized-bed) better preserve quality and shorten time, but they require reliable, affordable heat sources and appropriate dryer design. Multiple studies confirm that solar or sun drying tends to reduce curcuminoids and volatile oils relative to controlled hot-air approaches, whereas optimized hot-air/fluidized drying better maintains color and antioxidant capacity (Llano et al. 2022; Naik et al. 2020; Qamar et al. 2025).

Within Pakistan, turmeric is concentrated in specific districts (e.g., Kasur and parts of Okara in Punjab), where producers still report practical challenges with hygienic, weather-proof drying and volatile market returns after processing which underscores the value of low-cost, quality-preserving drying technologies (Ashraf et al. 2021; Government of Pakistan. 2023). Figure 1 shows the scenario of turmeric production in Pakistan and its export to other countries. Provincial statistics show concentrated turmeric area and output in the Lahore division, while sectoral reporting highlights Kasur as a dominant pocket; economic assessments further document processing constraints and price instability that incentivize on-farm value addition if appropriate technologies exist (Ashraf et al. 2023; Saeed et al. 2017). More broadly, Pakistan's post-harvest loss challenge remains substantial because of limited mechanization, energy costs, and inadequate infrastructure for controlled processing. Recent policy briefs and reviews note 20–40% losses in perishables and call for efficient, energy-aware technologies that suit smallholders and local conditions, precisely the context where efficient dryers can matter (FAO. 2024; Ghafoor et al. 2022).

Extensive research work has evaluated turmeric curing and drying methods. Reviews and experiments converge on two messages: (i) pretreatments (e.g.,

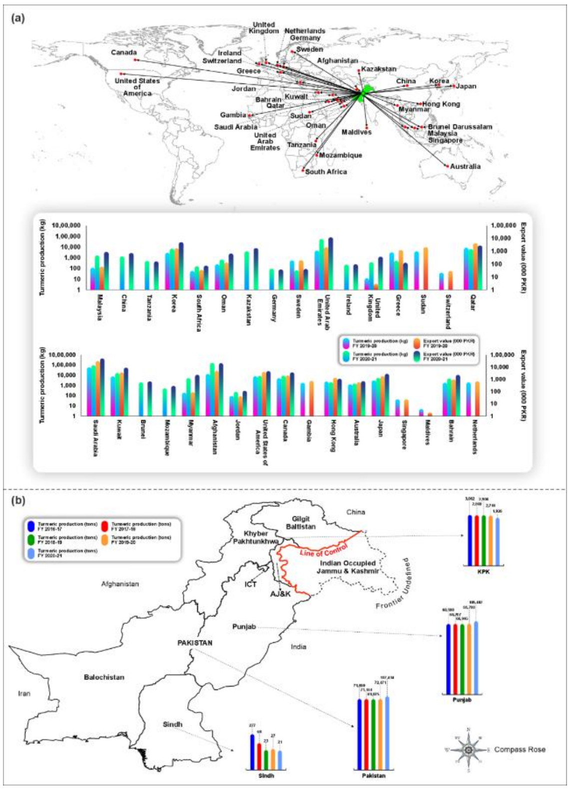

Figure 1. Current scenario of turmeric production and export in Pakistan (a) turmeric export across the globe, production, and export value, and (b) turmeric production in provinces.

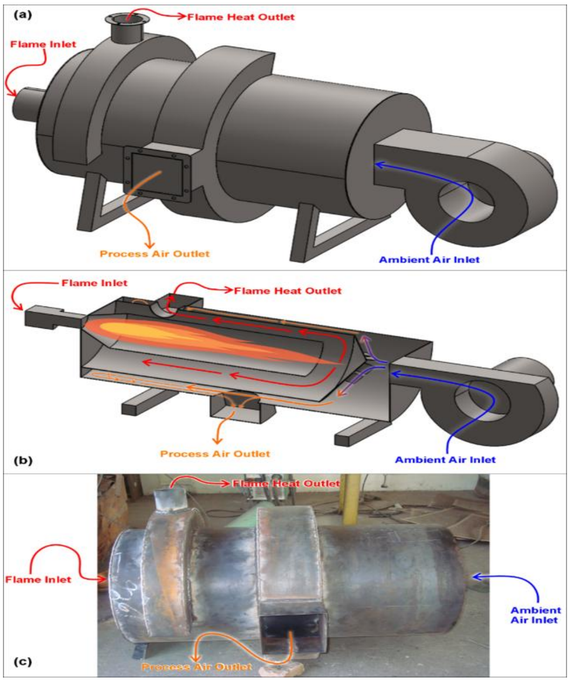

Figure 2. Illustration of the (a) 3D model, (b) flow diagram & working principle, and (c) developed fired–heat exchanger.

boiling/curing) influence color and drying kinetics; and (ii) controlled thermal environments (50–80 °C hot-air or fluidized-bed) can deliver superior color and curcumin retention versus open-sun, if air distribution and residence time are well managed. These findings derive from India and international studies, but they are broadly applicable to Pakistan's climatic and market realities (Llano et al. 2022; Thul & Shirsat. 2021). However, while solar tunnel and hybrid dryers have been piloted in Pakistan for fruits, mainstream adoption in spices like turmeric remains limited, often due to heat supply variability and the operating cost of reliable thermal systems. This points to the heat-source and heat-transfer subsystem as a strategic lever for improving dryer performance while containing costs (Anwar et al. 2010).

Figure 3. Experimental diesel–fired heat exchanger based turmeric dryer.

Figure 4. Generalized flow diagram of the CFD modeling process used in this study.

Fired heat exchangers (FHEs), with radiant and convective sections inside a firebox, are standard in process industries for converting combustion heat into controlled hot air/fluids, often with finned surfaces to raise the effective transfer area. Properly designed, the radiant section leverages flame radiation, and the convection section recovers sensible heat from flue gas; configurations include box-type and cylindrical heaters. These fundamentals translate well to agricultural dryers that need stable, uniform hot air at modest temperatures (Ibrahim & Al-Qassimi. 2013; Nadeem et al. 2022). For agriculture, indirect biomass or gas-fired furnaces coupled to heat exchangers have shown practical promise: flue gases are kept separate from the airstream product, and locally available fuels (e.g., rice husk, wood residues) can reduce operating costs. Demonstrations and evaluations, from the Philippines to South Asia, report acceptable drying efficiencies and significant cost advantages using indirect biomass-fired systems sized for smallholders (Khan et al. 2024; Khan et al. 2025; Prabhu et al. 2023; R. Sumner et al. 1983). Critically, Pakistan's rice sector has already flagged the value of better heat-exchange integration. In crossflow rice dryers, gas-fired units delivered higher drying rates and airflows than rice-husk-fired units, with authors explicitly recommending that the rice husk option "be improved by incorporating an appropriate heat exchanger." This is a direct, context-relevant signal that fired heat-exchange design is the limiting factor for biomass-based dryers in Pakistan (Ahmad et al. 2014; Qamar et al. 2024).

In fired equipment, computational fluid dynamics (CFD) is widely used to visualize flame structure, flue-gas recirculation, heat-flux distribution on tubes, and potential hot spots, inputs that translate directly into safer, more uniform, and more efficient heater/heat-exchanger designs. Applied studies in fired heaters and heat-exchanger modules show that CFD can guide burner configuration, fin layout, baffle cuts, and flow distribution to improve thermal effectiveness and reduce fuel use (Abeykoon. 2021; Fayyaz et al. 2024). CFD has been extended to biomass-fired grain dryers, where validated 3D models identified stagnant zones, flow maldistribution, and strategies (geometry tweaks, mixing/recirculation) that improved drying uniformity and time. That work underscores the practical value of CFD-informed modifications in small-scale, biomass-fired systems, however it has not yet been translated to turmeric dryers or to the fired heat-exchanger stage that feeds them (Delele et al. 2023; Hannan et al. 2024).

Altogether, the literature shows that (i) open-sun turmeric drying is quality- and hygiene-limited; controlled hot-air drying preserves quality but needs reliable, cost-efficient heat (Llano et al. 2022; Saha et al. 2022), (ii) indirect fired, biomass/gas systems can supply such heat; Pakistan's own studies on rice dryers specifically call for better heat-exchanger design (Ahmad et al. 2014; Jinjin et al. 2024), and (iii) CFD-guided design is mature in fired heaters and has shown benefits in biomass dryers, yet there is no reported, Pakistan-focused study that designs, develops, and experimentally validates a low-cost fired heat exchanger tailored to turmeric drying, air-side distribution quality, cost and energy efficiency (Delele et al. 2023; Romana & Shafae. 2023).

Figure 5. (a) sketch of turmeric curing pan, (b) in–field turmeric curing method, and (c) turmeric loaded onto the trays for drying in the dryer.

Therefore, the primary aim of this study was to design, develop and evaluate the thermodynamic performance of a cost-saving, diesel-fired heating exchanger aimed specifically to dry turmeric in Pakistan. The performance of the dryer was evaluated in terms of mobilized drying kinetics, thermal efficiency and operational economics, for uncrushed and crushed rhizomes. The second aim was to confirm the experimental findings by using Computational Fluid Dynamics (CFD) to simulate the air movement and heat transfer in the system.

Figure 6. Crushed turmeric sample (after boiling/curing).

Table 1. Design specifications of the developed fired heat exchanger based turmeric dryer.

Parameter	Unit
Type of machine	Tractor trailed behind
Overall length (mm)	5,000
Overall height (mm)	2,500
Overall width (mm)	1,850
Length of drying chamber (mm)	2,340
Width of drying chamber (mm)	1,570
Height of drying chamber (mm)	1,800
Type of heat exchanger	Double pipe cross flow type
Length of heat exchanger (mm)	1,150
Length of hitch (mm)	1,270
Tray size (mm x mm)	750 x 750
Height between two consecutive trays (mm)	133
Plenum height (mm)	320
Wheels diameter (mm)	630
Heating source	40-W diesel burner
Type of fan	Centrifugal blower
Flow of fan (m^3/s)	1.7
Blower drive mechanism	Pulleys and belts
Source of power	5 hp electric motor or engine
Drying capacity (kg)	1,000

Table 2. Parameters for determining adiabatic flame temperature.

Parameter	Unit	Equation
Specific heat of carbon dioxide, $c_{p(CO_2)}$	kJ/k mol K	$2.401 + (8.735 \times 10^{-3})T - (6.607 \times 10^{-6})T^2 + (2.002 \times 10^{-9})\, T^3$,
Specific heat of water vapors, $c_{p(H_2O)}$	kJ/k mol K	$4.07 - (1.108 \times 10^{-3})T + (4.152 \times 10^{-6})T^2 - (2.964 \times 10^{-9})\, T^3 + (0.807 \times 10^{-12})\, T^4$,
Specific heat of nitrogen gas, $c_{p(N_2)}$	kJ/k mol K	$3.675 - (1.208 \times 10^{-3})T + (2.324 \times 10^{-6})\, T^2 - (0.632 \times 10^{-9})\, T^3 - (0.226 \times 10^{-12})\, T^4$,
Enthalpy of carbon dioxide, $\Delta H_{f(CO_2)}$	kJ/mol	–393522
Enthalpy of water vapors, $\Delta H_{f(H_2O)}$	kJ/mol	–241827
Enthalpy of light diesel, $\Delta H_{f(C_{10}H_{20})}$	kJ/mol	6020
Enthalpy of reactants, $\Delta H_{\ (Reactants)}$	kJ/mol	–12373
Flame temperature, T	K	2410

Table 3. Constant parameters for heat transfer inside the shell.

Constant	Unit	Value
Stephen Boltzmann constant, σ	W/m^2 K	5.67E-08
Emissivity of mild steel, $\mathcal{E}$	–	0.45
Relative effectiveness factor of shield, α_{shld}	–	1
Relative effectiveness factor, α	–	0.45
Exchange factor, F	–	0.94
Thermal conductivity of mild steel, k	kJ/m K s	45.3
Convective heat transfer coefficient, h_o	kJ/m^2 K s	33
Convective heat transfer coefficient between process fluid and inside wall of tube, h_i	kJ/m^2 K s	3.5
Fouling factor of mild steel, R_f	m^2 K W^{-1}	0.0006

Table 4. Heat transfer through radiation and condition (shell side).

Constant	Unit	Value
Length of flame, L	m	0.535
Diameter of flame, D	m	0.14
Temperature at datum, T_{datum}	K	298
Temperature of gas, T_i	K	517
Quantity of light diesel used, m_f	kg/s	2.5
Mass of fuel, m_{fuel}	kg/s	0.14
Specific heat of fuel, $c_p, fuel$	kJ/kmolK	1.75
Net calorific value of fuel, NCV	kJ/kg	43,000
Mass of air, m_{air}	kg/s	2.076
Specific heat of air, c_p, air	kJ/kmolK	1.01
Mass of flue gases, m_{flue}	kg/s	0.842
Specific heat of flue gases, $c_p, flue$	kJ/kmolK	1.115
Radiant heat transfer, Q_r	kJ/s	105.32
Convective heat transfer in radiant section, Q_{conv}	kJ/s	28.54
Temperature of the inside wall, T_{wi}	K	507.65

Table 5. Heat transfer through conduction and convection (tube side).

Parameter	Unit	Value
Temperature outside the wall, T_{wo}	K	482.26
Convective heat transfer coefficient, U_c	W/m^2	3.22
Log Mean Temperature Difference, $LMTD$	K	292.12
Volumetric flow rate from blower, $Q_{\ v}$	m^3/s	0.95
Density of air, ρ	kg/m^3	1.225
Mass flow rate, m	kg/s	0.98
Temperature of air for drying, T_{air}	K	389

2. Materials and Methods

2.1. Development of turmeric dryer

The engineering design of the diesel fired–heat exchanger was calculated and completed in 3-dimensional assembly drawings in SOLIDWORKS. Details of the design of the diesel fired–heat exchanger are presented in Figure 2(a). Regarding the working principle of the diesel fired–heat exchanger, an elevated temperature is produced by burning fuel at the firebox/combustion chamber, which heats up the inside air as well as the combustion chamber. Hot gases (air) run through the shell and the other fluid (air) flows over the shell to transfer heat between the two fluids. Heat is transferred from one fluid to the other through the shell walls to the tube walls. The temperature inside the combustion unit reaches up to 400 °C. The produced heat is directly in contact with the heat exchanging device and heats up the heat exchanging device through conduction of heat. After transferring heat to the heat exchanger up to the rated value, the air and burnt gases are discharged through the hot air vent. The air to be heated is thrust to the outer surface of the shell through a distribution blower fan. The air gets heated in the furnace and is directed to the drying chamber through the outlet. Air velocity at the outlet is also lower than at the inlet of the diesel fired–heat exchanger. The flow diagram of diesel fired–heat exchanger is shown in Figure 2(b).

The diesel fired–heat exchanger was designed and developed at Agricultural Engineering Institute, National Agricultural Research Center, Islamabad. Diesel was selected as the fuel for this prototype due to its widespread availability in rural Pakistan, ease of handling, and ability to provide consistent and controllable heat output, critical for maintaining turmeric quality during drying. Biomass alternatives, while more sustainable, often require preprocessing, storage space, and specialized feeding systems, which were beyond the scope of this initial design phase. Figure 2(c) illustrates the developed diesel fired–heat exchanger. It consists of a combustion box (shell), a tube, oil burner, fuel injection pump, blower, and flue gas vent. Mild steel material was used for manufacturing the diesel fired–heat exchanger. The inner and outer surface diameters of tube were 0.48 m and 0.484 m, respectively and length of the tube was 1.035 m. A 2-hp single-phase motor was used with belt arrangement to drive the blower. Fins were provided on the outer side of shell to increase its surface area for better heat transfer through air convection. Flue gases were exited from a vent provided in the end section of the shell. This was a single-phase heat exchanger, i.e., the used fluid was air. A turmeric drying chamber was also developed. The heat exchanger was attached to the drying chamber. Figure 3 shows the developed diesel–fired heat exchanger based turmeric dryer. Table 1 presents the design specifications of the developed fired heat exchanger based turmeric dryer.

2.2. Design of heat exchanger

2.2.1 Flame temperature

Adiabatic flame temperature is an important parameter in designing the diesel fired–heat exchanger as the total energy input depends on the fuel used for burning inside it. Combustion results in formation of carbon dioxide (CO_2), nitrogen (N) and water vapors (Ibrahim et al. 2013; Zia et al. 2023). Actual flame temperature is always lower than theoretical temperature as complete combustion and perfect mixing of flame only occurs theoretically. Light diesel is a mixture of hydrocarbons and the general equation for its combustion is given as Equation 1. The parameters required for the estimation of adiabatic flame temperature are presented in Table 2.

$$C_{10}H_{20} + 15(O_2 + 3.76N_2) \rightarrow 10\ CO_2 + 10\ H_2O + 57\ N_2 \quad (1)$$

The change in enthalpy (ΔH) expressed in kJ units is equal to the sum of enthalpy changes in the reaction as well as the rising temperature of gases is shown as Equation 2.

$$\Delta H = \Delta H_{Reaction} + \Delta H_{Gases} \tag{2}$$

The relations of enthalpy change of reaction and gases are shown in Equations 3 and 4, respectively.

$$\Delta H_{Reaction} = 10\Delta H_{f_{(CO_2)}} + 10\Delta H_{f_{(H_2O)}} + 57\Delta H_{f_{(N_2)}} - \Delta H_{f_{(C_{10}H_{20})}} - 15\Delta H_{f_{(O_2)}} - 57\Delta H_{f_{(N_2)}} \tag{3}$$

$$\Delta H_{Gases} = \sum n \int_{298}^{T} c_p dT \tag{4}$$

where c_p is the specific heat of products (kJ/kg K). The evolutions of specific heat (c_p) expressed in (kJ/kg-K) of CO_2, H_2O and N_2 with temperatures are shown in Equations 5 through 7, respectively.

$$c_{p_{(CO_2)}} = 24.01 + (8.735 \times 10^{-2})\,T - (6.607 \times 10^{-5})\,T^2 + (2.002 \times 10^{-8})\,T^3 \tag{5}$$

$$c_{p_{(H_2O)}} = 40.07 - (1.108 \times 10^{-2})\,T + (4.152 \times 10^{-5})\,T^2 - (2.964 \times 10^{-8})\,T^3 + (0.807 \times 10^{-11})\,T^4 \tag{6}$$

$$c_{p_{(N_2)}} = 209.475 - (6.88 \times 10^{-2})\,T + (1.324 \times 10^{-4})\,T^2 - (3.602 \times 10^{-8})\,T^3 - (1.288 \times 10^{-11})\,T^4 \tag{7}$$

The specific heat of products was determined using Equation 8.

$$c_{p(Products)} = 10\,c_{p_{(CO_2)}} + 10\,c_{p_{(H_2O)}} + 57\,c_{p_{(N_2)}} \tag{8}$$

Extrapolating the coefficients of $c_{p_{(CO_2)}}$, $c_{p_{(H_2O)}}$, and $c_{p_{(N_2)}}$ in Equation 8 given as Equation 9.

$$c_{p(Products)} = 273.55 + 0.185 \times 10^{-2}T - 2.32 \times 10^{-5}T^2 - 4.56 \times 10^{-8}\,T^3 - 0.481 \times 10^{-11}\,T^4 \tag{9}$$

Integrating Equation 9 results in Equation 10.

$$\int_{298}^{T} c_p dT = \int_{298}^{T} 273.55 dT + \int_{298}^{T} (0.185 \times 10^{-2})\,T\,dT - \int_{298}^{T} (2.32 \times 10^{-5})T^2\,dT - \int_{298}^{T} (4.56 \times 10^{-8})\,T^3\,dT - \int_{298}^{T} (0.481 \times 10^{-11})\,T^4\,dT \tag{10}$$

Following the first law of thermodynamics, the heat content of the reaction and gases should always be the same as given in Equation 11.

$$0 = \Delta H_{Reaction} + \Delta H_{Gases} \tag{11}$$

Solving Equation 10 results in Equation 12 by summing and integrating the total heat content and specific heat of product gases which allows the calculation of adiabatic temperature using trial and error method (Tyagi. 2006).

$$273.55\mathrm{T} + (0.0925 \times 10^{-2})T^2 - (0.77 \times 10^{-5})T^3 - (1.14 \times 10^{-8})T^4 - (0.096 \times 10^{-11})T^5 - 93677 = 0 \tag{12}$$

2.2.2. Shell temperature

Inside the shell, the effective gas temperature depends on the length and the diameter of the flame. The effective gas temperature was estimated using the following relation given in Equation 13.

$$T_g = (\frac{q_f}{\varepsilon\sigma})^{1/4} \tag{13}$$

Determination of radiant heat flux from the flame in the diesel–fired heat exchanger is compulsory for computing the inside temperature in the shell. Shell temperature was determined by using the Shokri and Beler model (Ufuah & Bailey. 2011) as shown in Equation 14. For simplicity of calculations, the flame shape is taken as a regular body. In this case, we assumed the rectangular shape of the flame.

$$q_f = 15.4(\frac{L}{D})^{-1.59} \tag{14}$$

2.2.3. Heat transfer inside the shell

In radiant section, the heat of combustion is the total heat released by the burner (Q_{rls}), heat of air (Q_{air}) and heat of fuel (Q_{fuel}). Of all the heat radiated through combustion (Q_{comb}) is then absorbed in radiant section by radiant heat Q_r on tubes and shield area (Q_{shld}) whereas the remaining heat is lost through flue gases (Q_{flue}). Constants for the numerical calculation of heat transfer inside the shell are presented in Table 3.

$$Q_{in} = Q_{comb} = Q_{rls} + Q_{air} + Q_{fuel} \tag{15}$$

Inside the diesel–fired heat exchanger, heat is produced through combustion of fuel and air.

$$Q_{rls} = m_{fuel} \times NCV \quad (16)$$

where NCV is the net calorific value of fuel (kJ/kg). The heat of fuel and air are given in Equations 17 and 18, respectively.

$$Q_{fuel} = m_{fuel} \times c_{p(fuel)} \times (T_{fuel} - T_{datum}) \quad (17)$$

$$Q_{air} = m_{air} \times c_{p(air)} \times (T_{air} - T_{datum}) \quad (18)$$

Radiant heat (Q_R) produced inside the shell is transmitted through thermal emission, radiation, and convection in different parts of the diesel fired–heat exchanger as given in Equation 19.

$$QR=Qr+Qconv \quad (19)$$

The radiant heat transfer follows the relationship given in Equation 20.

$$Qr=\sigma\times\alpha\times Acp\times F\times(Tg4-Twi4) \quad (20)$$

where T_{wi} is the wall temperature which can be determined using Equation 21 developed by (Couper et al. 2012).

$$T_{wi} = 100 + 0.5(T_1 - T_2) \quad (21)$$

Radiant heat is used to heat up walls of diesel fired–heat exchanger and then to transmit heat outside the diesel fired–heat exchanger through convective process. Cengel et al. (Çengel & Ghajar. 2020)described Equation 22 for determination of convective heat transfer in radiant section and Equation 23 for determining heat of shield section.

$$Q_{conv} = h_c \times A_t \times (T_g - T_{wi}) \quad (22)$$

$$Q_{shld} = \sigma \times \alpha \times (A_{cp} \times F)_{shld} \times (T_g^4 - T_{wi}^4) \quad (23)$$

Exchange factor for single pass in diesel fired–heat exchanger was calculated using graph between Prandtl, Reynold numbers and exchange factor (Çengel et al. 2020). During heat transfer process in diesel fired–heat exchangers it is assumed that 60% heat is lost in the radiant section: 10% through convection and 5% during conduction process. Ibrahim et al. (Ibrahim et al. 2013) assumed 5% heat losses during combustion of fuel as given in Equation 24. The heat of flue gases is determined using Equation 25. The calculated heat transfer through radiation and conduction (shell side) is presented in Table 4.

$$Q_{losses} = 5\% \times m_{fuel} \times NCV \quad (24)$$

$$Q_{flue} = m_{flue} \times c_{p(flue)} \times (T_g - T_{datum}) \quad (25)$$

Conduction heat transfer (Q_{cond}) occurs from the shell side to the tube side through the thickness of the surface using conduction Equation 26.

$$Q_{cond} = \frac{kA(T_{wi} - T_{wo})}{d} \quad (26)$$

where k is conduction coefficient, T_{wi} is the temperature of inside wall (K) and T_{wo} is the temperature of outside wall (K) and d is the thickness of the wall (m). After conduction, the convective heat transfer (Q_{conv}) is determined across the diesel fired–heat exchanger using Equation 27.

$$Q_{conv} = U_c \times A_c \times LMTD \quad (27)$$

where U_c is the convective heat transfer coefficient (W/m^2) and $LMTD$ is the log-mean temperature difference across both temperatures (K). The overall heat transfer coefficient is the function of fluid properties and composition of materials in diesel fired–heat exchanger. The overall heat transfer coefficient can be determined by using convection heat transfer coefficient between inside and outside the wall and the process fluid. Theoretical resistance to heat flow due to its corrosion is fouling resistance (R_f) and for mild steel its value is 0.0006 m^2-K/W (Kreider & White. 2017). The relation given in Equation 28 explained by (Cao. 2010) is used to determine the overall convection heat transfer coefficient, U_c.

$$\frac{1}{U_c} = \frac{1}{hi} + \frac{1}{ho} + R_f \quad (28)$$

The blower fan forced air in convection section of the diesel–fired heat exchanger. This air absorbed the convective heat from outside the shell and entered the drying chamber for drying of agricultural produce as given in Equation 29 and 30, respectively.

$$m = Q_v \times \rho \quad (29)$$

$$T_{air} = \frac{q}{m \times c_p} + T_{amb} \tag{30}$$

where, m is the mass flow rate of air (kg/s), Q_v is the volumetric flow rate of air (m^3/s), ρ is the density of air (kg/m^3), T_{amb} is the ambient air temperature, q is convection heat (kJ/s) transferred in the drying chamber, c_p is the specific heat of air and T_{air} is the temperature of final heated air (K). The calculated heat transfer through conduction and convection (tube side) is presented in Table 5.

2.2.4. Heat balance

There are three sources of heat input, viz., heat released by burner (Q_{rls}), heat of combustion air (Q_{air}) and sensible heat of fuel (Q_{fuel}). The heat is transferred from flame to inside shell surface by two heat transfer methods, viz. radiant heat, and convection heat. The heat is taken out from the shell by the heat absorbed by the shell (Q_R) , shield heat (Q_{shld}), heat losses (Q_{losses}) and sensible heat of the flue gases (Q_{flue}). Ibrahim et al. (Ibrahim et al. 2013) balanced diesel fired–heat exchanger using the following equations from Equations 31 through 33. The heat energy balance of the diesel fired–heat exchanger is presented in Table 6.

$$Q_{in} = Q_{out} \tag{31}$$

$$Q_{in} = Q_{comb} = Q_{rls} + Q_{air} + Q_{fuel} \tag{32}$$

$$Q_{out} = Q_R + Q_{conduction} + Q_{shld} + Q_{losses} + Q_{flue} \tag{33}$$

2.2.5. Effectiveness

In the design of the diesel fired–heat exchanger, maximum energy of hot fluid must be transferred to the cold fluid. The amount of energy transferred is called effectiveness and is considered an important parameter for performance assessment. To find the effectiveness (ε) of diesel fired–heat exchanger, it is necessary to determine the available energy for both fluids.

$$Q_h = m_h c_h (T_{hi} - T_{ho}) = C_h (T_{hi} - T_{ho}) \tag{34}$$

$$Q_c = m_c c_c (T_{co} - T_{ci}) = C_c (T_{co} - T_{ci}) \tag{35}$$

where, c_h and c_c are heat capacities of hot and cold sides given as the product of mass and specific heat. Ideally, heat energy delivered must be equal to heat energy absorbed by the fluid.

$$Q_h = Q_c \tag{36}$$

Fakheri (Fakheri. 2006) used Equation 37 for determining the effectiveness of diesel fired–heat exchanger. The magnitude of Q_{max} can be determined by using Equation 38.

$$\varepsilon = \frac{Q}{Q_{max}} \tag{37}$$

$$Q_{max} = C_{min}(T_{hi} - T_{ci}) \tag{38}$$

2.3. Computational fluid dynamics

Model selection is one of the most critical parameters to compute heat exchanger (Wilcox. 1998). Therefore, choosing a suitable Computational Fluid Dynamics (CFD) model for simulating heat exchanger system entails considering the system's features, the physics involved, the computational resources available, and the level of precision necessary. A steady-state CFD analysis was performed using the standard k-epsilon (k-ε) turbulence model to predict airflow and heat transfer within the heat exchanger. While this approach provides a reliable approximation of average thermal behavior, it does not capture time-dependent variations. Future work will incorporate transient simulations to better represent dynamic drying conditions. The k-ε model is selected based on its accuracy in literature (Ghazanfari et al. 2023; Kuzmin et al. 2007; Zhang et al. 2023). The k-ε turbulence model is widely recognized as the predominant CFD model for determining average flow properties in turbulent flow scenarios. The model is based on two transport equations, which are often referred to as partial differential equations (PDEs). These equations are used to describe turbulence in a comprehensive manner. The turbulent kinetic energy (k) is the main variable that is conveyed, while the rate of dissipation of turbulent kinetic energy (ε) is the secondary variable that is transferred. The main premise of this model is that turbulent viscosity is isotropic, which implies that the amount of Reynolds stress corresponding to deformation rate is constant in any direction. The core k- turbulence model was developed by Launder and Spalding in 1974. Based on our present understanding of the essential processes, the standard k- turbulence model is preferred for its practicality, since it minimizes uncertainty and provides a set of formulas that can be used in diverse turbulent scenarios. The exact k- equations, on the other hand, include an abundance of factors that are both unpredictable and difficult to measure. The k-model was created expressly to consider plane shearing layer and looping flows. The reason for its importance lies in its frequent use and validation as a turbulence model, which finds use in various industrial and environmental flow scenarios. It is commonly beneficial in situations with limited fluid movement, where the Reynolds shear stresses play a crucial role, as well as in flows characterized by free-shear layers and little pressure gradients. A generalized flow diagram of the modeling process in this study is presented in Figure 4 which consists of the following steps: geometry development, material assigning, selection the simulation model, defining the CFD goals, creating meshing of the 3D model, perform the simulations and gain results, post-processing of the results and perform any optimization if needed.

The continuity equation (Andersson et al. 2011; Rodriguez. 2019; Wong & Heryanto. 2004) was used in the CFD simulations to examine the mass, momentum, and energy related to the flow, which illustrates the law of conservation of mass in a regulated volume, given as Equation 39.

$$\frac{\partial \rho u}{\partial x_{i,j,k}} = 0 \tag{39}$$

where, ρ is fluid density (kg/m^3) and u_j is flow velocity in m/s. The mass and momentum conservation are given by Equations 40 and Equation 41.

$$\frac{\partial \rho}{\partial t} + \frac{\partial}{\partial x_j}(\rho u_j) = 0 \tag{40}$$

$$\frac{\partial \rho u_t}{\partial t} + \frac{\partial \rho u_i u_j}{\partial x_j} = -\frac{\partial p}{\partial x_i} + \frac{\partial \sigma_{ij}}{\partial x_j} \text{standardk} + F_i \tag{41}$$

The turbulent kinetic energy and dissipation rate available in (DS SolidWorks. 2015; Sobachkin & Dumnov. 2013) are given by Equations 42 to 45.

$$\frac{\partial}{\partial t}(\rho k) + \frac{\partial y}{\partial x_i}(\rho k u_i) = \frac{\partial}{\partial x_j}\left[\left(\mu + \frac{\mu_t}{\sigma_k}\right)\frac{\partial k}{\partial x_j}\right] + \tau_{ij}^R \frac{\partial u_i}{\partial x_j} - \rho\varepsilon + \mu_t P_B \tag{42}$$

$$\frac{\partial}{\partial t}(\rho \varepsilon) + \frac{\partial y}{\partial x_i}(\rho \varepsilon u_i) = \frac{\partial}{\partial x_j}\left[\left(\mu + \frac{\mu_t}{\sigma_\varepsilon}\right)\frac{\partial \varepsilon}{\partial x_j}\right] + C_{\varepsilon 1}\frac{\varepsilon}{k}\left(f_1 \tau_{ij}^R \frac{\partial u_i}{\partial x_j} + C_B \mu_t P_B\right) - f_2 C_{\varepsilon 2} \rho \frac{\varepsilon^2}{k} \tag{43}$$

$$\tau_{ij} = \mu s_{ij}, \tau_{ij}^R = \mu_t s_{ij} - \frac{2}{3}\rho k \delta_{ij}, s_{ij} = \frac{\partial u_i}{\partial x_j} + \frac{\partial u_j}{\partial x_i} - \frac{2}{3}\delta_{ij}\frac{\partial u_k}{\partial x_k} \tag{44}$$

$$P_B = -\frac{g_i}{\sigma_B}\frac{1}{\rho}\frac{\partial \rho}{\partial x_i} s \tag{45}$$

where, P_b shows the buoyancy effect which illustrates the change in temperature with respect to space, where C_μ =0.09, $C_{\varepsilon 1}$ = 1.44, $C_{\varepsilon 2}$ =1.92, σ_k =1, σ_ε =1.3, σ_B =0.9, and C_B =1. The heat flux and heat transfer in solid media (DS SolidWorks. 2015; Sobachkin et al. 2013) is given by Equation 46 and Equation 47, respectively.

$$q_t = \left(\frac{\mu}{Pr} + \frac{\mu_t}{\sigma_c}\right)\frac{\partial h}{\partial x_i}\frac{\partial \rho}{\partial t} + \frac{\partial}{\partial x_j}(\rho u_j) = 0 \tag{46}$$

$$\frac{\partial \rho e}{\partial t} = \frac{\partial}{\partial x_i}\left(\lambda_i \frac{\partial T}{\partial x_i}\right) + Q_H \tag{47}$$

where, q_t shows the heat flux, Pr shows the Prandtl number, h shows the enthalpy, σ_c =0.90, e is the specific internal energy, Q_H is the heat emitted per unit volume, and λ_i is the thermal conductivity tensor.

2.4. Turmeric treatments

2.4.1. T1 – boiling (curing)

Performance of turmeric dryer was evaluated at a farmer's field in Daoke Khaniana Kot Dogran, Kasur, Punjab, Pakistan. Before drying, the turmeric rhizomes must be cured. This involves boiling the roots to soften them and to remove the raw odor. However, the boiling time must not be so extended else color of the rhizomes may deteriorate. If the boiling time is too short, the rhizomes may be brittle. Therefore, turmeric rhizomes were boiled for 40–50 minutes. A normal hemispherical pan of about 1,400 mm diameter was used to boil turmeric as shown in Figure 5(a) and Figure 5(b). The boiling capacity of the pan was about 300 kg per batch. Crop residues were used as fuel for heating the furnace. In this experiment, the turmeric was cured in the pan without prior washing.

The cured turmeric was spread on the ground to drain the free water. The turmeric was loaded onto trays (10 kg turmeric on each) and placed in the drying chamber (Figure 5c). A total of 600 kg of turmeric was loaded in the drying chamber, although the drying capacity of the dryer was 1,000 kg/batch. However, for data collection purposes and ease of experiment, only 600 kg turmeric was loaded.

2.4.2. T2 – boiling (curing) and crushing

In industrial drying of turmeric, turmeric is first sliced or crushed using a slicing machine after boiling and then dried in a dryer. This process reduces the drying time significantly. Therefore, in this part of the experiment, about 7.5 kg of turmeric was crushed manually after boiling and put in the drying chamber. It is worth mentioning that the turmeric was not sliced using a knife, however it was crushed or broken into irregular pieces by manual labor, shown in Figure 6. Turmeric was crushed to understand the comparative performance of the dryer between the conventional way of drying (only boiling/curing) and boiling/curing and crushing.

3. Results and Discussion

The fired–heat exchanger was tested to compare the results with the theoretical results. For this purpose, data of ambient air temperature, wet bulb temperature, ambient humidity, heated air temperature and heated air humidity were collected. Data was analyzed using PsycPro® software.

3.1. Heat transfer

The minimum theoretical air required for combustion of diesel was calculated to be 14.8 kg of air per kg of diesel fuel. The stoichiometric air required for complete combustion of diesel was determined to be 16 kg of air per kg of diesel fuel. By performing trial and error method of Equation 12, the adiabatic flame temperature was calculated by using equation developed by integration method. The obtained adiabatic flame temperature was 2410 K. This result was a bit higher than the previous findings (Ibrahim et al. 2013) which reported 2128 K was the actual flame temperature. This deviation may be attributed to the computation method, as using slightly different parameters can yield different results.

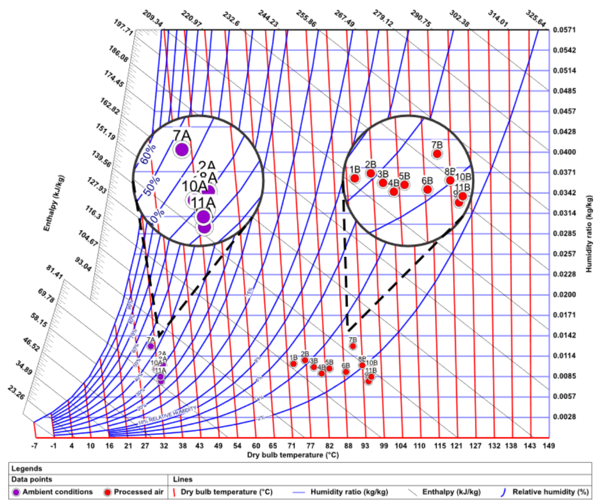

Figure 7. Psychrometric performance profile of the fired heat exchanger.

The diameters of inner and outer sides of the tube were 0.48 m and 0.484 m, respectively with wall thickness of 0.004 m. The volumetric flow rate of air impacting the tube was 0.8 m^3/s and the mass flow rate (Q_m) and velocity of air (V_a) through effective area were calculated to be 2.076 kg/s and 4.35 m/s, respectively. The calculated radiant heat flux from the flame was 1.82 kW/m^2. All values were put in Equation 13 to calculate the inside temperature in the shell, which was 244 °C. The rate of energy available in the shell and the rate of energy lost from the tube were found to be 220.26 and 108.12 kW, respectively. Heat from the flame is distributed in the shell through radiation and convection process and it comes out of the shell through conduction process. The amount of heat transferred through the radiation process was 221.12 kJ and the useful heat at the end of convection section was 108.11 kJ. The heated air temperature after passing through the fired–heat exchanger was 96.8 °C. This heat was used for heating air which was further utilized for drying agricultural produce.

Table 6. Heat energy balance (kJ/s) in diesel–fired heat exchanger.

Parameter	Value
Heat released by burner, Q_{rls}	29.86
Sensible heat of fuel, Q_{fuel}	517.64
Sensible heat of combustion air, Q_{air}	459.82
Total heat transfer to radiant shell, Q_R	113.70
Radiant heat to shield, Q_{shld}	106.57
Conductive heat transfer, Q_{cond}	221.63
Convective heat transfer, Q_{conv}	108.11
Assumed heat losses, Q_{loses}	211.97
Heat in gases leaving radiant section, Q_{flue}	247.44

3.2. Psychrometric analysis and losses

Temperature and relative humidity play a vital role in the drying process. Low relative humidity and high air temperature removes more moisture from the wet product. The psychometric analysis of fired–heat exchanger was carried out to check its air heating performance. The data of the heat exchanger were collected for 30 minutes and plotted on psychometric chart using PsycPro® software. The results revealed that the fired–heat exchanger could increase the air temperature up to 96.8 °C and decrease relative humidity to 1.62%, which can successfully dry many agricultural commodities (given in Table 7). Figure 7 shows the psychrometric profile of the thermodynamic performance of the fired–heat exchanger. At dry bulb temperature of 96.8 °C of the process air, actual vapor pressure was 10.95 mmHg, and the relative humidity was 1.62%. In Figure 7, the datapoints move from A to B (symbolizing sensible heating process in the fired–heat exchanger) which depicts that temperature of the air is increasing, and relative humidity is decreasing with negligible change in absolute humidity as on heating the air, no moisture can enter in it from surroundings. Corresponding to the process air conditions above, the ambient dry bulb temperature and relative humidity were 33.5 °C and 28.2%, which upon passing through the heat exchanger changed to 96.8 °C and 1.62 %, respectively. The fired–heat exchanger provided constant temperature in the drying chamber (average 89.3 °C), resulting in rapid and quality dried products when attached to a drying chamber.

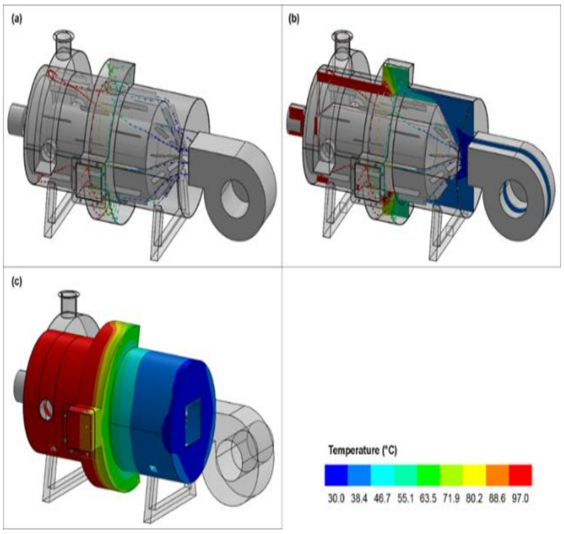

Figure 8. CFD-based profile of (a) flow trajectories corresponding to the air temperature, (b) cross–sectional cut–plot of the variation in the air temperature, and (c) surface plot of the change in temperature of air inside the fired–heat exchanger.

In the designed fired–heat exchanger, ambient air was allowed a single pass over the heated surface, which resulted in low contact time for heat transfer. The average temperature of flue gases was 190 °C, which can be reduced by passing the ambient air multiple times over the heated surface to increase the contact time.

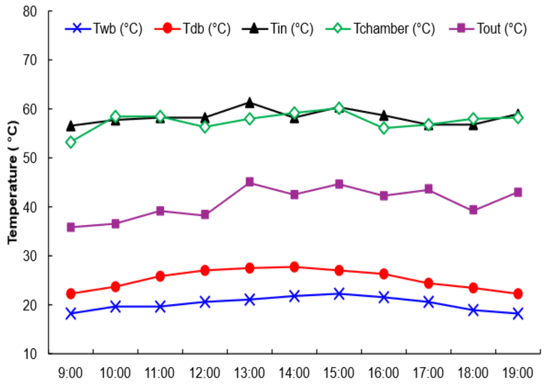

Figure 9. Temperature profile of experimental drying performance of fired heat exchanger-based dryer for uncrushed and boiled/cured turmeric.

The surface temperature of the outer pipe was about 40-45 °C which can be reduced by covering it with optimum thickness of insulation material. Difference in the theoretical and experimental results could be attributed to the higher heat losses from the mild steel material compared to ideal adiabatic conditions.

3.3. CFD simulation

The CFD simulation scrutinized the performance of a diesel-fired heat exchanger featuring fins on the flame tube, executed using the SOLIDWORKS Flow Simulation module. The heat source, in this case, emanated from a diesel flame situated within the inner tube, where the fin configuration was also accounted for in the heat source body. This design choice aims to amplify the contact surface area, thereby intensifying heat transfer efficiency. Figure 8 illustrates the CFD-based profile of (a) flow trajectories corresponding to the air temperature, (b) cross–sectional cut–plot of the variation in the air temperature, and (c) surface plot of the change in temperature of air inside the fired–heat exchanger.

For inlet boundary conditions, an air velocity of 4.35 m/s was applied proximately to the fan blower. The ambient air entering the system was characterized by a temperature of 30 °C, along with a relative humidity of 50%. Outlet boundary conditions emulated environmental parameters, with a pressure set at 101325 Pa, and air maintained at 30 °C and 50% relative humidity. The heat exchanger's material composition was specified as mild steel alloy, a common choice in such applications. A thoroughly constructed mesh was employed to discretize the computational domain, ensuring robust numerical analysis. Upon conducting the simulation, a noteworthy observation emerged. The outlet temperature closely approximated 96 °C, aligning closely with experimental findings. Nevertheless, a striking disparity manifested in the distribution of high-temperature air. Contrary to expectations, a concentration of elevated temperature air was observed at the far end of the exchanger, contrary to the anticipated uniform distribution. In addition, flow trajectories, crucial indicators of fluid behavior, elucidated this phenomenon. Figure 8(a) illustrates the flow trajectories corresponding to the air temperature.

The airflow emanating from the blower fan toward the outlet exhibited comparatively lower temperature than the air circulating from the far end of the exchanger. This discrepancy could be attributed to the augmented surface contact area and prolonged contact time experienced by air circulating from the far end. This discrepancy in non–uniform distribution of air temperature could be further observed from the cut–plot (Figure 8(b)), and surface–plot (Figure 8(c)). These results underscore the intricate interplay of design parameters, fluid dynamics, and heat transfer mechanisms in the performance of diesel–fired heat exchangers with fin configurations. Further investigations into flow patterns and heat distribution profiles hold promises for refining the design and operational efficiency of such systems. These findings suggest that while the CFD model reliably predicts overall thermal behavior, localized variations require further

Table 7. Experimental results obtained from the fired–heat exchanger at different time steps.

Test No.	$Ta_{(db)}$ (°C)	$Ta_{(wb)}$ (°C)	RHa (%)	$Tp_{(db)}$ (°C)	RHp (%)
1	33.5	21	32.3	73	4.71
2	34	21.5	32.9	76.5	4.26
3	33	20.5	31.8	79	3.52
4	33.5	20	28.2	81.2	2.93
5	33.5	20.5	30.3	83.6	2.86
6	33	20	29.7	88.5	2.26
7	31	22	45.8	91	2.83
8	34	21	30.8	93.5	2.05
9	33	19	25.6	95.1	1.52
10	32	20	32.7	96.2	1.76
11	33	19.5	27.6	96	1.58
12	34	21.5	32.9	96.7	1.95
13	34	22	35	95.8	2.14
14	33.5	21.5	34.5	96.2	2.02
15	33.5	20	28.2	96.8	1.62

T stands for temperature (°C), **RH** stands for relative humidity (%), **a** represents ambient air, **p** stands for process air, **db** stands for dry bulb, and **wb** stands for wet bulb.

Table 8. Moisture take-off analysis of the drying chamber during drying of uncrushed and boiled/cured turmeric.

Time (hours)	Lower 20 trays moisture take-off (kg)	Middle 20 trays moisture take-off (kg)	Upper 20 trays moisture take-off (kg)	Total moisture take-off (kg)
0	0	0	0	0
2	12.18	11.99	11.26	35.43
4	12.18	11.99	11.26	35.43
6	11.12	10.79	10.07	31.99
8	11.12	10.79	10.07	31.99
10	9.32	9.11	8.06	26.49
12	9.32	9.11	8.06	26.49
14	11.65	10.15	9.55	31.35
16	13.98	11.19	11.04	36.22
18	7.63	7.67	7.58	22.88
20	7.63	7.67	7.58	22.88
22	10.53	10.63	10.12	31.28
24	13.43	13.59	12.65	39.67
26	10.17	7.19	6.16	23.52
28	10.17	7.19	6.16	23.52
30	5.28	7.60	7.42	20.29
32	-	8.01	8.67	16.68
34	-	-	9.48	9.48
Total	**155.72**	**154.70**	**155.19**	**465.61**

refinement in geometry and flow distribution.

3.4. Turmeric drying profiles

3.4.1. T1 – boiled (cured) turmeric

Figure 9 and Figure 10 illustrate the temperature and relative humidity profiles of the drying performance of the developed dryer in case of uncrushed and boiled/cured turmeric, respectively. According to the results, the average wet bulb temperature (Twb) during the test period was 20.2 °C and the average ambience temperature (Tdb) was 25.3 °C. The average ambient relative humidity (RHamb) of the air was calculated as 50.0%. The average temperature (Tin) and relative humidity (RHin) of hot air exiting the heat exchanger and going into the drying chamber were determined as 58.4 °C and 11.9%, respectively.

Table 9. Temperature drop, wet bulb depression of the drying air and drying efficiency of the dryer during uncrushed and boiled/cured turmeric drying.

Time	$Ta_{(wb)}$ (°C) (A)	$Ta_{(db)}$ (°C) (B)	Tchamber (°C) (C)	Tout (°C) (D)	Tdrop (°C) (E=C–D)	$Tdepression_{(wb)}$ (°C) F=(C–A)	η (%) ($G = \frac{E}{F} \times 100$)
09:00	18.13	22.25	53.25	35.75	17.50	35.13	49.82
10:00	19.63	23.75	58.50	36.50	22.00	38.88	56.59
11:00	19.75	25.88	58.50	39.08	19.43	38.75	50.13
12:00	20.50	27.13	56.25	38.25	18.00	35.75	50.35
13:00	21.13	27.63	58.00	45.00	13.00	36.88	35.25
14:00	21.88	27.75	59.25	42.50	16.75	37.38	44.82
15:00	22.19	27.00	60.25	44.63	15.63	38.06	41.05
16:00	21.50	26.25	56.00	42.25	13.75	34.50	39.86
17:00	20.50	24.50	56.75	43.50	13.25	36.25	36.55
18:00	18.88	23.50	58.00	39.25	18.75	39.13	47.92
19:00	18.33	22.17	58.33	43.00	15.33	40.00	38.33
Average	**20.22**	**25.25**	**57.55**	**40.88**	**16.67**	**37.34**	**44.61**

$Ta_{(wb)}$ stands for wet bulb temperature of ambient air, **$Ta_{(db)}$** represents dry bulb temperature of ambient air, **Tchamber** stands for chamber temperature, **Tout** stands for exit temperature, **Tdrop** stands for temperature drop of the drying air, **$Tdepression_{(wb)}$** stands for wet bulb depression of drying air and **η** stands for drying efficiency of the dryer.

The drying chamber temperature (Tchamber) and relative humidity (RHchamber) were determined as 57.5 °C and 20.3%, respectively. It is worth mentioning that the air temperature right at the inlet of the drying chamber was about 1°C higher than the temperature inside the drying chamber due to the reason that after entering the plenum unit of the dryer, the hot air expands to the full width of the plenum which causes slight reduction in temperature (as observed). The average exit air temperature (Tout) was calculated as 43.5 °C and the relative humidity (RHout) was determined as 35.4%. For a quick observation, the ambient air was heated from 25.2 °C to 58.4 °C in the heat exchanger.

Moisture content (MC) of the turmeric samples was determined every couple of hours by measuring the weight of the samples. It was noted that the MC of lower trays' samples, which was close to the hot air plenum, decreased faster than the middle and upper trays' samples, respectively. This behavior is logical because the hot air entering the drying chamber first absorbs the moisture from lower trays and then moves upward. The initial MC of uncrushed and boiled/cured turmeric was determined as 80%. It was observed that the rate of MC removal was quite low at the start of the experiment whereas gradually it increased rapidly. Figure 11 illustrates the moisture content reduction profile of the uncrushed and boiled/cured turmeric. The final MC of 10% was attained in the lower, middle and upper trays' samples in 30, 32 and 34 hours, respectively, for a batch of 600 kg of turmeric. It is worth mentioning that the lower sample trays were removed after 30 hours, and the middle and upper trays were later moved in the lower positions. This presents a limitation of improper circulation of hot air at the bottom plenum. Providing another hot air plenum at the front side of the dryer may address this limitation, to some extent, for rationed supply of hot air in each row of turmeric trays. However, this approach may increase the drying time. Otherwise, uniform drying in the drying chamber may be attained by shuffling the upper trays with the lower ones which may need additional time and labor. Evidently, 10% MC in the lower trays' samples was attained in the first 30 hours of the experiment, however, at this time, the MC of middle and upper trays' samples was calculated about 25% and 36%, respectively. The moisture take-off by the hot air from the lower, middle and upper portion of the dryer is present in Table 8.

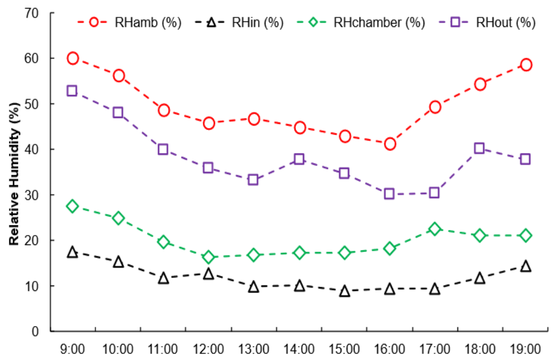

Figure 10. Relative humidity profile of experimental drying performance of fired heat exchanger-based dryer for uncrushed and boiled/cured turmeric.

From the batch load of 600 kg at 80 % initial moisture content, a total of 466 kg of moisture/water was removed to bring it down to a moisture content of 10 %. The weight of dried turmeric remained only 134 kg. On an average, the dryer removed 13.7 kg of moisture content from turmeric every hour. The total drying time was 34 hours for this batch.

Table 9 presents the temperature drop of the heated air while passing through the layers of turmeric, wet bulb temperature, wet bulb depression of drying air and drying efficiency of the dryer during turmeric drying at different times of the day. It should be noted that wet bulb depression is the difference between the dry bulb temperature of drying air and the wet bulb temperature, whereas the temperature drop of the drying air is the difference between the dry bulb temperature of the drying air and dry bulb temperature of the exit air. Evidently, it was found that the drying efficiency has a strong correlation with the temperature drop in the dryer. The drying efficiency varied from 35.25% to 56.59% at different times of the day. The greater the difference between chamber air and the exit air, the greater was the drying efficiency of the dryer. For instance, the highest temperature drop recorded was 22 °C at 10:00 hours coincidently the drying efficiency was also highest at this time i.e., 56.6%. The average efficiency of the dryer was 44.6%. It can be stated that by achieving a temperature drop of higher than 22°C, approximately more than 57% dryer efficiency could be achieved.

The cost of turmeric dryer is a combination of the fixed cost and variable cost. Fixed costs include depreciation, interest in average investment and repair and maintenance cost, whereas the variable cost includes labor cost, fuel cost and lubricant cost. A complete cost analysis of turmeric dryer for turmeric drying is presented in Table 10. Evidently, the total annual fixed cost per ton of drying turmeric was Rs.4,427 and for a batch of 600 kg, it was Rs. 2,656. The variable cost per batch of 600 kg of drying turmeric was Rs. 30,112. It should be noted that the fixed cost per batch of turmeric drying was estimated by assuming the drying capacity of the dryer @ 30 tons per year. By combining the fixed and the variable costs, the total cost of drying 600 kg of turmeric was estimated as Rs. 32,768 which leads to the cost of drying one kg of turmeric Rs. 55. The unit cost of drying uncrushed turmeric was not widely accepted by the local turmeric farming community, which may lead to a limitation of constrained adoption of the developed technology for drying whole turmeric rhizomes (roots). On the other hand, by using this technology, farmers can save their crop produce from wastage due to weather, which deteriorates the quality of the product due to aflatoxins and fungus which are the major reasons of least acceptance of Pakistani turmeric in the international market.

3.4.2. T2 – boiled (cured) and crushed turmeric

Results of crushed turmeric are shown in Table 11. The total time for drying crushed turmeric samples was only 8 hours. The initial MC of 80% was decreased to 10% in 8 hours. Profile of moisture content reduction is shown in Figure 12. Although, the time and cost of drying (presented in Table 12) of crushed turmeric was significantly reduced compared to whole turmeric rhizomes, however the crushed

Table 10. Cost analysis of turmeric dryer by conventional boiling/curing method.

Basic parameters	**Cost (Rs.)**
Purchase price (Rs.)	800,000
Useful life (Years)	10
Salvage value 10% of purchase price (Rs.)	80,000
Annual fixed cost	
Depreciation (Purchase price – Salvage value) / Useful life in years	72,000
Interest 12% on average investment = (Purchase price + Salvage value)/2*12%	52,800
Repair and maintenance (1% of Purchase price)	8,000
Total annual fixed cost	132,800
Annual turmeric drying capacity (tons/year)	30
Fixed cost of drying per ton of turmeric	4,427
Fixed cost of drying a batch of 600 kg of turmeric	2,656
Variable cost	
Labor cost for loading, unloading and operating the dryer (4 man-hours per batch) (Rs.)	600
Diesel cost of one batch of 600 kg (3Lx34 hours) Rs. 280/L (Rs.)	28,560
Lubricant cost (10% of engine fuel consumption, 1 L/h) = 34x10%=3.4LxRs. 280/L (Rs.)	952
Total variable cost (Rs.)	30,112
Total fixed and variable cost for drying one batch of 600 kg turmeric (Rs.)	32,768
Total cost for drying one kg of uncrushed turmeric (Rs.)	**55**

Table 11. Moisture take-off and drying profile of boiled/cured and crushed turmeric.

Time (hours)	**Weight (kg)**	**Moisture take-off (kg)**	**Moisture content (%)**
0	7.34	0	80
1	6.44	0.90	77.20
2	5.60	0.84	73.79
3	4.78	0.82	69.29
4	4.03	0.75	63.57
5	3.35	0.68	56.18
6	2.75	0.60	46.62
7	2.18	0.57	32.66
8	1.63	0.55	9.94

Table 12. Cost analysis of turmeric dryer by conventional boiling/curing method.

Basic parameters	**Cost (Rs.)**
Purchase price (Rs.)	800,000
Useful life (Years)	10
Salvage value 10% of purchase price (Rs.)	80,000
Annual fixed cost	
Depreciation (Purchase price - Salvage value) / Useful life in years	72,000
Interest 12% on average investment = (Purchase price + Salvage value)/2 *12 %	52,800
Repair and maintenance (1% of Purchase price)	8,000
Total annual fixed cost	132,800
Annual turmeric drying capacity (tons/year)	50
Fixed cost of drying per ton of turmeric	2,656
Fixed cost of drying a batch of 600 kg of turmeric	1,594
Variable cost	
Labor cost for loading, unloading and operating the dryer (8 man-hours per batch) (Rs.)	1,200
Cost of diesel for one batch of 600 kg (3Lx8 hours) Rs. 280/L (Rs.)	6,720
Lubricant cost (10 % of engine fuel consumption, 1 L/h) = 8x10%=0.8LxRs. 280/L (Rs.)	224
Total variable cost (Rs.)	8,144
Total fixed and variable cost for drying one batch of 600 kg turmeric (Rs.)	9,738
Total cost for drying one kg of crushed turmeric (Rs.)	**16**

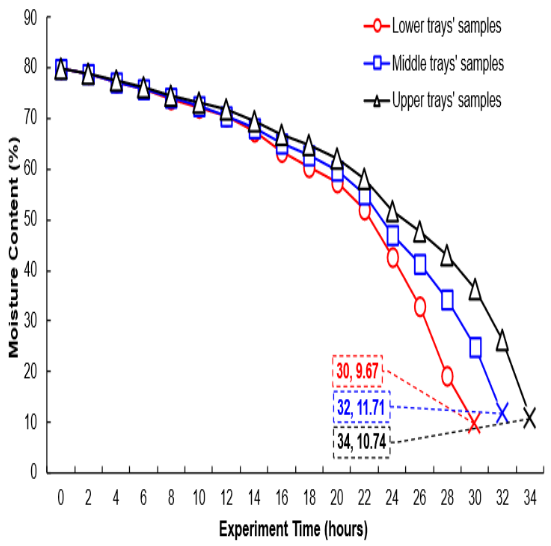

Figure 11. Moisture content reduction profile of uncrushed and boiled/cured turmeric.

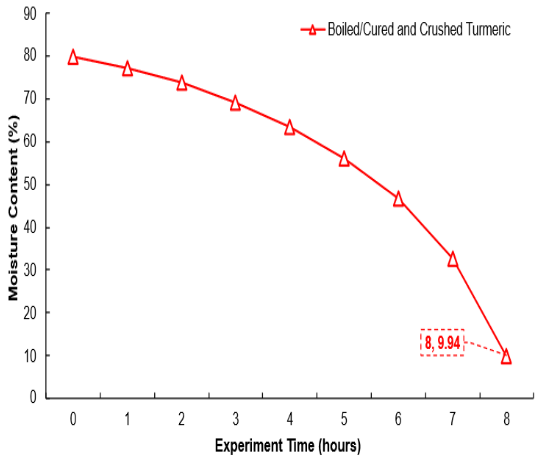

Figure 12. Moisture content reduction profile of boiled/cured and crushed turmeric.

turmeric has least acceptance in the local market. This reduced social acceptance can be linked with the fact that crushed turmeric needs to be further processed as soon as possible to protect it from deterioration and mites/insects, whereas the whole turmeric rhizomes can be stored for approximately 3–6 years and can be ground and packed on demand. In general, the quality of the whole dried turmeric has not deteriorated over the years. On the other hand, the shelf life of crushed turmeric is comparatively small. Therefore, farmers and suppliers tend to dry the whole uncrushed turmeric. This is a limit which can be averted by creating awareness among the stakeholders of further process (i.e., grinding and packing) crushed turmeric for export purposes.

Cost analysis of drying crushed turmeric is shown in Table 12. Evidently, the drying cost of 600 kg batch can be reduced from Rs. 32,768 to Rs. 9,738 (for crushed turmeric), approximately 30% lower than the conventional whole turmeric rhizome drying method.

The cost of drying of one kg of turmeric was reduced from Rs. 55 to Rs. 16 after crushing. This unit cost of drying is widely acceptable by the local farmers however the adoption of crushing before drying is still limited and required awareness campaigns and further processing.

4. Conclusions

A fired heat exchanger-based dryer was successfully designed, developed, and evaluated for turmeric drying at farm level. The system was intended to handle one-ton batches; however, field trials were conducted on 600 kg of uncrushed turmeric, reducing moisture from 80% to 10% in 34 hours. The average drying efficiency was 45%, with a drying cost of PKR 55 per kg. In contrast, crushed turmeric dried to 9.94% moisture in only 8 hours, achieving a fourfold faster drying rate and reducing the cost to PKR 16 per kg. These results highlight the significant influence of particle size on drying kinetics and economics. The developed dryer demonstrated technical feasibility for both uncrushed and crushed turmeric, though operational costs for whole rhizomes remain high. Future improvements should focus on enhancing heat exchanger efficiency through double-pass flue gas flow and integrating biomass-based fuel options to reduce fuel consumption and improve sustainability.

Acknowledgements

This research was funded by Public Sector Development Programme (PSDP), Government of Pakistan, under the project titled Research for Agricultural

Development Program (RADP), awarded to Pakistan Agricultural Research Council (PARC). This study was conducted at the Agricultural Engineering Institute (AEI), National Agricultural Research Centre (NARC), Islamabad.

Conflicts of Interest

The authors declare no conflicts of interest.

Author contributions

Hafiz Sultan Mahmood: Conceptualization, Formal analysis, Investigation, Methodology, Project administration, Writing – original draft. Asif Ali Mirani: Data curation, Investigation, Project administration, Resources, Supervision, Validation. Badar Munir Khan Niazi: Data curation, Methodology, Software, Visualization, Writing – review & editing. Hadeed Ashraf: Formal analysis, Methodology, Software, Validation, Visualization, Writing – review & editing. Muzammil Husain: Data curation, Formal analysis, Resources, Visualization, Writing – review & editing. Hafiz Md-Tahir: Data curation, Methodology, Resources, Validation, Writing – review & editing.

Reference

Abeykoon, C. (2021, May 21-23). *Modelling of Heat Exchangers with Computational Fluid Dynamics* Proceedings of the 8th International Conference on Fluid Flow, Heat and Mass Transfer (FFHMT'21), Canada. https://doi.org/10.11159/ffhmt21.127

Ahmad, M., Mirani, A. A., Mahmood, H. S., Ahmad, T., & Saeed, M. A. (2014). Performance Evaluation of Cross-Flow Rice Dryers. *Pakistan Journal of Agricultural Research*, *27*(4), 277-286. https://www.cabidigitallibrary.org/doi/pdf/10.5555/20153118424

Andersson, B., Andersson, R., Håkansson, L., Mortensen, M., Sudiyo, R., & Van Wachem, B. (2011). *Computational fluid dynamics for engineers*. Cambridge university press.

Anwar, T., Tahir, S., & Ahmad, I. (2010). A Simple Solar Drying Technology with Special Reference to Farm Level Chilli Drying in Sindh Province of Pakistan. *International Journal of Biology and Biotechnology*, *7*(1-2), 53-58. https://ftp.asianindexing.com/article.php?jid=406&id=194772

Ashraf, H., Qamar, S., Riaz, N., Shamshiri, R. R., Sultan, M., Khalid, B., Ibrahim, S. M., Imran, M., & Khan, M. U. (2023). Spatiotemporal Estimation of Reference Evapotranspiration for Agricultural Applications in Punjab, Pakistan. *Agriculture*, *13*(7), 1388. https://doi.org/10.3390/agriculture13071388

Ashraf, H., Sultan, M., Shamshiri, R. R., Abbas, F., Farooq, M., Sajjad, U., Md-Tahir, H., Mahmood, M. H., Ahmad, F., Taseer, Y. R., Shahzad, A., & Niazi, B. M. K. (2021). Dynamic Evaluation of Desiccant Dehumidification Evaporative Cooling Options for Greenhouse Air-Conditioning Application in Multan (Pakistan). *Energies*, *14*(4), 1097. https://doi.org/10.3390/en14041097

Cao, E. (2010). *Heat Transfer in Process Engineering* (1st Edition ed.). McGraw-Hill Education. https://www.accessengineeringlibrary.com/content/book/9780071624084

Çengel, Y. A., & Ghajar, A. J. (2020). *Heat and Mass Transfer: Fundamentals and Applications* (6th Edition ed.). McGraw Hill Education. https://books.google.com.pk/books?id=1YPhoAEACAAJ

Couper, J. R., Penney, W. R., Fair, J. R., & Walas, S. M. (2012). 8 - Heat Transfer and Heat Exchangers. In J. R. Couper, W. R. Penney, J. R. Fair, & S. M. Walas (Eds.), *Chemical Process Equipment (Third Edition)* (pp. 161-221). Butterworth-Heinemann. https://doi.org/10.1016/B978-0-12-396959-0.00008-2

Delele, M. A., Mihret, Y. C., & Mellmann, J. (2023). Performance evaluation and improvement of prototype rice husk fueled mixed flow rough rice dryer using CFD model. *Drying Technology*, *41*(15), 2447-2463. https://doi.org/10.1080/07373937.2023.2252056

DS SolidWorks. (2015). *Introducing SolidWorks*. D. S. SolidWorks. https://my.solidworks.com/solidworks/guide/SOLIDWORKS_Introduction_EN.pdf

Fakheri, A. (2006). Heat Exchanger Efficiency. *Journal of Heat Transfer*, *129*(9), 1268-1276. https://doi.org/10.1115/1.2739620

FAO. (2024). *Agricultural mechanization for smallholder farmers in Pakistan: Results of a multistakeholder policy dialogue – Policy brief*. Food and Agriculture Organization of the United Nations. https://doi.org/10.4060/cd1865en

Fayyaz, U., Hannan, A., Naqvi, S. Q. A., Ahmad, B., Asif, M., Ashraf, H., & Qamar, S. (2024, February 28-29). *A16-On the Effective Use of Water Absorbing Agents for Enhanced Performance of Wheat Yield and Growth in Rainfed Areas* Two-Days National Conference on Climate Change and Water Resources (CCWR) Bridging the Gap for SDG6, Multan, Pakistan. https://www.researchgate.net/profile/Saad-Zaheer-5/publication/383410278_Two-Days_National_Conference_on_Climate_Change_and_Water_Resources_CCWR_Bridging_the_Gap_for_SDG6_Proceedings_of_the_National_Conference_on_Climate_Change_and_Water_Resources_CCWR_Bridging_the_Gap_for/links/66cb68c097265406eaad014f/Two-Days-National-Conference-on-Climate-Change-and-Water-Resources-CCWR-Bridging-the-Gap-for-SDG6-Proceedings-of-the-National-Conference-on-Climate-Change-and-Water-Resources-CCWR-Bridging-the-Gap-for.pdf#page=81

Ghafoor, A., Basher, M. A., Badar, H., & Lee, S. (2022). *Building Horticulture Value Chains and Reducing Postharvest Losses in Pakistan*. Asian Development Bank. https://doi.org/10.22617/BRF220545-2

Ghazanfari, V., Imani, M., Shadman, M. M., Amini, Y., & Zahakifar, F. (2023). Numerical study on the thermal performance of the shell and tube heat exchanger using twisted tubes and Al2O3 nanoparticles. *Progress in Nuclear Energy*, *155*, 104526. https://doi.org/10.1016/j.pnucene.2022.104526

Government of Pakistan. (2023). *Fruit, Vegetables and Condiments Statistics of Pakistan*. Ministry of National Food Security and Research Government of Pakistan. https://mnfsr.gov.pk/SiteImage/Misc/files/draft_fvc_1_0.pdf

Hannan, A., Shoaib, M., Naqvi, S. Q. A., Ahmad, B., Ashraf, H., Qamar, S., & Asif, M. (2024, February 28-29). *A57-Comparative Analysis of Soft Computing Approaches for Rainfall–Runoff Modeling: A Case of Tarbela Dam* Two-Days National Conference on Climate Change and Water Resources (CCWR) Bridging the Gap for SDG6, Multan, Pakistan.

Ibrahim, H. A.-H., & Al-Qassimi, M. M. (2013). Calculation of Radiant Section Temperatures in Fired Process Heaters. *Chemical Engineering and Science*, *1*(4), 55-61. https://doi.org/10.12691/ces-1-4-2

Jinjin, W., Niazi, S., Saeed, T., Naz, M., & Hussain, S. (2024). Wheat Yield Under Climate Change: Effect of Temperature and Wind Speed on the Crop Life Cycle and Productivity Estimated by DSSAT-Icsim Model *Journal of Food and Agricultural Technology Research*, *3*(1). https://doi.org/10.69501/a8bxs979

Kanwal, R., Ashraf, H., Sultan, M., Babu, I., Yasmin, Z., Nadeem, M., Asghar, M., Shamshiri, R. R., Ibrahim, S. M., Ahmad, N., Imran, M. A., Zhou, Y., & Ahmad, R. (2020). Effect of 1-Methyl Cyclopropane and Modified

Atmosphere Packaging on the Storage of Okra (Abelmoschus esculentus L.): Theory and Experiments. *Sustainability*, *12*(18), 7547. https://doi.org/10.3390/su12187547

Khan, A. A., Haq, Z.-U.-., Asam, H. M., Khan, M. A., Zeeshan, A., Qamar, S., & Saad, A. (2024). Performance Evaluation of Half-Feed Rice Combine Harvester *Proceedings of the Pakistan Academy of Sciences: A. Physical and Computational Sciences*, *61*(1), 858. https://doi.org/10.53560/PPASA(61-1)858

Khan, A. A., Haq, Z. U., Qamar, S., Zeeshan, A., Khan, M. A., Saad, A., Raza, S. M., Islam, M. A., Ahmad, I., Ali, M., & Waqas, A. (2025). Performance Evaluation and Comparison of Ride-on and Walk-after Rice Transplanters. *Pakistan Journal of Science*, *77*(01), 27-32. https://doi.org/10.57041/vol77iss01pp27-32

Kreider, M., & White, G. (2017). 12 - Thermal performance degradation and heat-transfer fouling. In J. Riznic (Ed.), *Steam Generators for Nuclear Power Plants* (pp. 365-404). Woodhead Publishing. https://doi.org/10.1016/B978-0-08-100894-2.00014-5

Kuzmin, D., Mierka, O., & Turek, S. (2007). On the implementation of the κ-ε turbulence model in incompressible flow solvers based on a finite element discretisation. *International Journal of Computing Science and Mathematics*, *1*(2-4), 193-206. https://doi.org/10.1504/IJCSM.2007.016531

Llano, S. M., Gómez, A. M., & Duarte-Correa, Y. (2022). Effect of Drying Methods and Processing Conditions on the Quality of Curcuma longa Powder. *Processes*, *10*(4), 702. https://doi.org/10.3390/pr10040702

Nadeem, M. U., Waheed, Z., Ghaffar, A. M., Javaid, M. M., Hamza, A., Ayub, Z., Nawaz, M. A., Waseem, W., Hameed, M. F., Zeeshan, A., Qamar, S., & Masood, K. (2022). Application of HEC-HMS for flood forecasting in hazara catchment Pakistan, south Asia. *International Journal of Hydrology* *6*(1), 7-12. https://doi.org/10.15406/ijh.2022.06.00296

Naik, B. K., Joshi, M., Muthukumar, P., Sultan, M., Miyazaki, T., Shamshiri, R. R., & Ashraf, H. (2020). Investigating Solid and Liquid Desiccant Dehumidification Options for Room Air-Conditioning and Drying Applications. *Sustainability*, *12*(24), 10582. https://doi.org/10.3390/su122410582

Prabhu, N., Saravanan, D., & Kumarasamy, S. (2023). Eco-friendly drying techniques: a comparison of solar, biomass, and hybrid dryers. *Environmental Science and Pollution Research*, *30*(42), 95086-95105. https://doi.org/10.1007/s11356-023-28807-z

Qamar, S., Ashraf, H., Sultan, M., Ibrahim, S. M., & Khan, M. U. (2025). Data-Driven Irrigation Scheduling: A Spatiotemporal Assessment of Crop Water Requirements for Major Crops in Punjab, Pakistan. *Earth Systems and Environment*. https://doi.org/10.1007/s41748-025-00729-5

Qamar, S., Ashraf, H., Sultan, M., Shoaib, M., & Hannan, A. (2024, February 28-29). *A12-Exploring Decadal Spatiotemporal Trends in Reference Evapotranspiration and Dominant Climatic Factors in Punjab, Pakistan using Geospatial Analysis* Two-Days National Conference on Climate Change and Water Resources (CCWR) Bridging the Gap for SDG6, Multan, Pakistan.

R. Sumner, H., E. Sumner, P., C. Hammond, W., & E. Monroe, G. (1983). indirect-fired biomass furnace test and bomb calorimeter determinatinons. *Transactions of the ASAE*, *26*(1), 238-

0241. https://doi.org/10.13031/2013.33911

Rodriguez, S. (2019). *Applied Computational Fluid Dynamics and Turbulence Modeling: Practical Tools, Tips and Techniques*. Springer Nature. https://doi.org/10.1007/978-3-030-28691-0

Romana, N., & Shafae, G. (2023). Leveraging Nature's Arsenal, Biopesticidal Warriors: Randomising Melon Fruit Fly (Bacrocera Cucurbitae) In Bitter Gourd Culture, For Sustainable Control. *Journal of Food and Agricultural Technology Research*, *2*(2). https://doi.org/10.69501/a3abwv70

Saeed, R., Bashir, A., Khan, S. B., Bakhsh, K., & Qasim, M. (2017). An Economic Assessment of Turmeric Production in Punjab-Pakistan. *Pakistan Journal of Agriculture, Agricultural Engineering and Veterinary Sciences*, *33*(1), 85-99. https://pjaaevs.sau.edu.pk/index.php/ojs/article/view/87

Saha, G., Sharangi, A. B., Upadhyay, T. K., Al-Keridis, L. A., Alshammari, N., Alabdallah, N. M., & Saeed, M. (2022). Dynamics of Drying Turmeric Rhizomes (Curcuma longa L.) with Respect to Its Moisture, Color, Texture and Quality. *Agronomy*, *12*(6), 1420. https://doi.org/10.3390/agronomy12061420

Sobachkin, A., & Dumnov, G. (2013, 2013). Numerical basis of CAD-embedded CFD. https://www.solidworks.com/sw/docs/flow_basis_of_cad_embedded_cfd_whitepaper.pdf

Thul, P. P., & Shirsat, B. S. (2021). Effect of curing and drying process of turmeric on its quality: A review. *The Pharma Innovation*, *10*(3), 1017-1024. https://www.thepharmajournal.com/archives/2021/vol10issue3/PartN/13-5-92-294.pdf

Tyagi, P. (2006). *Thermochemistry*. Discovery Publishing House. https://books.google.com.pk/books/about/Thermochemistry.html

Ufuah, E., & Bailey, C. (2011). Flame radiation characteristics of open hydrocarbon pool fires. Proceedings of the World congress on Engineering. https://www.researchgate.net/publication/286061580_Flame_Radiation_Characteristics_of_Open_Hydrocarbon_Pool_Fires

Wilcox, D. C. (1998). *Turbulence modeling for CFD* (Vol. 2). DCW industries La Canada, CA. http://servidor.demec.ufpr.br/CFD/bibliografia/Carlos%20Eduardo%20Americo/Refer%C3%AAncias%20Carlos%20Eduardo/Wilcox2006.pdf

Wong, N. H., & Heryanto, S. (2004). The study of active stack effect to enhance natural ventilation using wind tunnel and computational fluid dynamics (CFD) simulations. *Energy and Buildings*, *36*(7), 668-678. https://doi.org/10.1016/j.enbuild.2004.01.013

Zhang, X., Ai, Q., & Wang, W. (2023). Effects of gas models on radiative heat transfer in the combustion chamber of a hydrogen gas turbine. *International Journal of Hydrogen Energy*, *48*(77), 30144-30155. https://doi.org/10.1016/j.ijhydene.2023.04.193

Zia, S. u. R., Ashraf, I., Hasan, G., & Asghar, S. (2023). Perception of Peri-Urban Vegetable Growers on the Use of Sewage Water for Irrigation Lahore, Punjab, Pakistan. *Journal of Food and Agricultural Technology Research*, *2*(2). https://doi.org/10.69501/262vpa93